


Article

Enhanced Ultraviolet Damage Resistance in Magnesium Doped Lithium Niobate Crystals through Zirconium Co-Doping

Tengfei Kong ¹, Yi Luo ², Weiwei Wang ³, Hanxiao Kong ⁴, Zhiqin Fan ^{1,*} and Hongde Liu ^{5,6,*} 

¹ School of Sciences, Henan University of Technology, Zhengzhou 450001, China; kongtf@haut.edu.cn

² Key Laboratory for Special Functional Materials of Ministry of Education, Henan University, Kaifeng 475004, China; luoy61@163.com

³ Department of Mathematics and Physics, Shijiazhuang Tiedao University, Shijiazhuang 050043, China; weiweiwang@mail.nankai.edu.cn

⁴ College of Chemistry and Environmental Science, Hebei University, Baoding 071002, China; konghxiao@163.com

⁵ MOE Key Laboratory of Weak-Light Nonlinear Photonics and School of Physics, Nankai University, Tianjin 300071, China

⁶ TEDA Institute of Applied Physics, Nankai University, Tianjin 300071, China

* Correspondence: lhdzfz@sina.com (Z.F.); liuhd97@nankai.edu.cn (H.L.)

Abstract: MgO-doped LiNbO₃ (LN:Mg) is famous for its high resistance to optical damage, but this phenomenon only occurs in visible and infrared regions, and its photorefractive is not decreased but enhanced in ultraviolet region. Here we investigated a series of ZrO₂ co-doped LN:Mg (LN:Mg,Zr) regarding their ultraviolet photorefractive properties. The optical damage resistance experiment indicated that the resistance against ultraviolet damage of LN:Mg was significantly enhanced with increased ZrO₂ doping concentration. Moreover, first-principles calculations manifested that the enhancement of ultraviolet damage resistance for LN:Mg,Zr was mainly determined by both the increased band gap and the reduced ultraviolet photorefractive center O^{2-/-}. So, LN:Mg,Zr crystals would become an excellent candidate for ultraviolet nonlinear optical material.

Keywords: lithium niobate; ultraviolet damage resistance; defects; first-principles calculations



Citation: Kong, T.; Luo, Y.; Wang, W.; Kong, H.; Fan, Z.; Liu, H. Enhanced Ultraviolet Damage Resistance in Magnesium Doped Lithium Niobate Crystals through Zirconium Co-Doping. *Materials* **2021**, *14*, 1017. <https://doi.org/10.3390/ma14041017>

Academic Editor: Daniel Vizman

Received: 19 January 2021

Accepted: 19 February 2021

Published: 21 February 2021

Publisher's Note: MDPI stays neutral with regard to jurisdictional claims in published maps and institutional affiliations.



Copyright: © 2021 by the authors. Licensee MDPI, Basel, Switzerland. This article is an open access article distributed under the terms and conditions of the Creative Commons Attribution (CC BY) license (<https://creativecommons.org/licenses/by/4.0/>).

1. Introduction

Lithium niobate (LiNbO₃, LN), also known as the silicon of nonlinear optics, is famous for its excellent physical properties such as acousto-optic, electro-optic, pyro-electric, piezoelectric, and nonlinear properties [1,2]. Although it has been grown for more than half a century, LiNbO₃ has remained one of the hot issues for researchers up to now [3]. In LiNbO₃, the optically-induced damage, also called the photorefractive, can be produced easily with a laser beam of several milliwatts, which seriously hinders its applications such as optical waveguides, frequency convertors, and Q-switches at high light intensities [4]. The good news is that doping MgO into LiNbO₃ solves this problem well, and the optical damage resistance for LiNbO₃ can be increased by two orders of magnitude, substantially promoting its practical use in nonlinear optics [5,6]. Nowadays, MgO doped LN (LN:Mg) still garners extensive research interest in optical waveguide, domain engineering, and quasi-phase-matching, however, it should be noted that most of these researches have only been carried out in visible and infrared regions, but not in ultraviolet (UV) [7,8]. In fact, LN:Mg exposes the visible enhancement of UV photorefractive [9], and this is a serious problem that has become a noteworthy impediment to its extension of applications into UV regions.

As we know, the chemical element Zr is considered as a unique and promising dopant in LiNbO₃ since it has a lower doping threshold (~2.0 mol.%) and a optimal distribution coefficient close to one, especially the strong optical damage resistance from UV to visible [10–13]. It should be pointed out that it has been the only doped LN crystal

possessing superior resistance against UV damage so far [14]. Generally, this property is thought to be related to the replacement of Zr^{4+} ions against Nb^{5+} on Li sites because the element Zr is adjacent to Nb in the periodic table. It has been reported that Zr^{4+} ions co-dope with some transition metal elements in LN crystals [15,16], such as Fe, Mn, Cu, and Ce, which can considerably reduce the light-induced scattering as well as improve the response speed. Besides, Zr doping also improves the near infrared emission efficiency in LN:Er, LN:Yb,Er crystals [17]; meanwhile, it can also stabilize the signal output of the Ti-diffused LN waveguides under the high-power pumping without optical damage observed [18]. Meanwhile, we have reported that some additional ZrO_2 doping into LN:Mg not only can finely adjust the phase-matching temperature but also realize the room temperature noncritical phase-matching [19]. The above research results suggest that Zr doping have such a strong impact on the properties of LN, so further research on its influence on the UV photorefraction of LN:Mg is very necessary and meaningful to promote the laser frequency conversion to UV wavelength region. Therefore, in this work we mainly investigated the resistance against UV damage of ZrO_2 co-doped LN:Mg crystals. Moreover, the first-principles calculations were employed to explore the effect of the crystal defect on the UV photorefractive properties in the doubly-doped LiNbO_3 .

2. Materials and Methods

A series of fixed 5.0 mol.% MgO and various ZrO_2 (0, 0.5, 1.0 and 1.5 mol.%) co-doped LiNbO_3 crystals were investigated and labelled as LN:Mg_{5.0}Zr_{0.5}, LN:Mg_{5.0}Zr_{1.0}, and LN:Mg_{5.0}Zr_{1.5}, respectively. For comparison, the 2.0 mol.% ZrO_2 -doped congruent LN crystal was also prepared, labeled as LN:Zr_{2.0}. Here, the crystal growth and treatment had been described in our previous report [19].

The transmitted beam spot distortion method [20] was performed directly and evaluated the optical damage resistance of crystals in the UV region. An *e*-polarized beam operating at 355 nm from a continuous wave frequency-tripled solid-state laser with a maximum output power of 100 mW was focused into the 3.0-mm-thick *y*-plates. The laser beam was polarized parallel to the *c*-axis of the plates, and the highest intensity at the focal point was $2.2 \times 10^5 \text{ W/cm}^2$. When a crystal suffers from the optical damage, the transmitted beam spot is smeared and elongated along the *c*-axis with decreased intensities at the central part. Moreover, in order to further characterize the optical damage resistance at 355 nm quantitatively, we also used the two-wave coupling holographic recording method [21], namely, two coherent *e*-polarized beams with irradiation intensities of 400 mW/cm^2 were focused into the *y*-oriented plates at the intersecting angle of 28° (2θ) to measure the light-induced refractive index changes (Δn) of these crystals.

In addition, to explore the linking mechanism between defect structure and optical damage resistance properties, the theoretical calculation for the defects and electronic structure of the crystals was performed by the Vienna Ab-initio Simulation Package (VASP) and general gradient approximation (GGA) [22,23]. The cutoff energy of the projector augmentation wave (PAW) pseudo-potentials was 400 eV with an allowed error in energy from relaxation of 10^{-5} eV. Moreover, the calculations of the bulk defects in perfect LN were carried out in the super-cell containing $2 \times 2 \times 1$ conventional unit cells with 120 atoms, meanwhile the employed $2 \times 2 \times 1$ *K*-points mesh over the Brillouin-zone was generated by the Monkhost–Pack scheme [24].

3. Results and Discussion

3.1. Resistance Against Ultraviolet Damage

Figure 1 depicts the images of the transmitted beam spots for different samples after 5 min radiation. With the ZrO_2 doping concentration increasing from 0.5 to 1.5 mol.%, no beam spot distortion is observed in LN:Mg,Zr crystals with a maximum light intensity of $2.2 \times 10^5 \text{ W/cm}^2$, as in the case of LN:Zr_{2.0}. For comparison, the transmitted light beam spot of LN:Mg_{5.0} obviously diffuses along the *c*-axis under the low light intensity of $2.8 \times 10^3 \text{ W/cm}^2$. Based on the results above, we found out that the resistance against

UV optical damage of LN:Mg_{5.0} is nearly improved by two orders of magnitude by only 0.5 mol.% ZrO₂ doping.

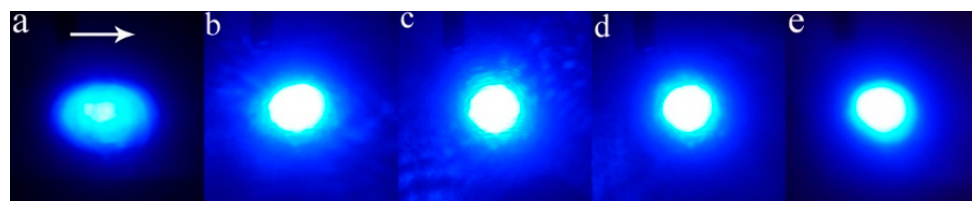


Figure 1. Distortion of transmitted laser beam spots after 5 min of irradiation. The white arrow represents the *c*-axis of the crystal. (a) LN:Mg_{5.0}; (b) LN:Mg_{5.0},Zr_{0.5}; (c) LN:Mg_{5.0},Zr_{1.0}; (d) LN:Mg_{5.0},Zr_{1.5}; (e) LN:Zr_{2.0}. The light intensities are (a) 2.8×10^3 W/cm² and (b–e) 2.2×10^5 W/cm².

We also calculated the refractive index changes by two-wave coupling holographic recording method, and the relevant results are shown in Figure 2. From this figure, it reveals that the changes of the refractive index of LN:Mg_{5.0} have lowered about an order of magnitude by co-doping with ZrO₂, which can even be compared with that of LN:Zr_{2.0}. Considering the inverse correlation in the change of refractive index with the optical damage resistance of the crystals, we conclude that the additional ZrO₂ dopants greatly reduce the UV optical damage of LN:Mg_{5.0}. However, it does not show a linear pattern between the refractive index changes and ZrO₂ co-doping with increasing ZrO₂ doping concentration in doubly crystals, and this particularity probably signifies that ZrO₂ doping has had a profound effect on the crystal structure of LN:Mg. So, we utilized the first-principles calculations to find out more about the inherent mechanism of enhanced UV optical damage resistance of LN:Mg by ZrO₂ co-doping.

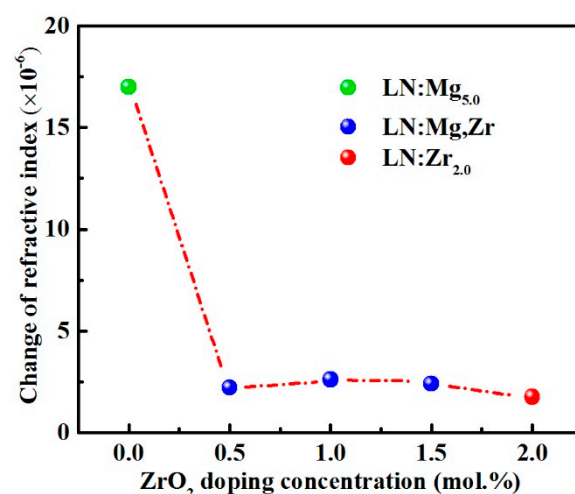


Figure 2. Refractive index changes of LN:Mg,Zr crystals as a function of ZrO₂ doping concentration. That of LN:Zr_{2.0} is labelled for comparison.

3.2. Defects Structure in the LN:Mg,Zr

Generally, the formation energy is treated as the stability criterion of defects in materials [25]. According to the optimization model of perfect LN [26], we firstly calculated the formation energies of point defects Mg_{Li}^+ , $\text{Mg}_{\text{Nb}}^{3-}$, $\text{Zr}_{\text{Li}}^{3+}$, $\text{Zr}_{\text{Nb}}^{3-}$ in LN:Mg,Zr to investigate the substitution sequence of doping ions, and the results are shown in Figure 3. It should be noted that the concentration increase of doping ions will cause the raise of Fermi level [27], so it can be observed from the figure that Mg_{Li}^+ and $\text{Zr}_{\text{Li}}^{3+}$ transform into $\text{Mg}_{\text{Nb}}^{3-}$ and $\text{Zr}_{\text{Nb}}^{3-}$ at the points when $E_F = 1.9$ eV and $E_F = 1.6$ eV, respectively, which illustrates that Mg^{2+} and Zr^{4+} ions give priority to form Mg_{Li}^+ and $\text{Zr}_{\text{Li}}^{3+}$ rather than $\text{Mg}_{\text{Nb}}^{3-}$ and $\text{Zr}_{\text{Nb}}^{3-}$. It is widely accepted [14] that doping ions in LN are assumed preferably to occupy Li sites and replace

anti-site $\text{Nb}_{\text{Li}}^{4+}$ up to the threshold value, and further above the threshold value, all $\text{Nb}_{\text{Li}}^{4+}$ defects are replaced, then doping ions separately enter Nb sites and Li sites. Clearly, Zr^{4+} ions occupy Nb sites ahead of Mg^{2+} ions.

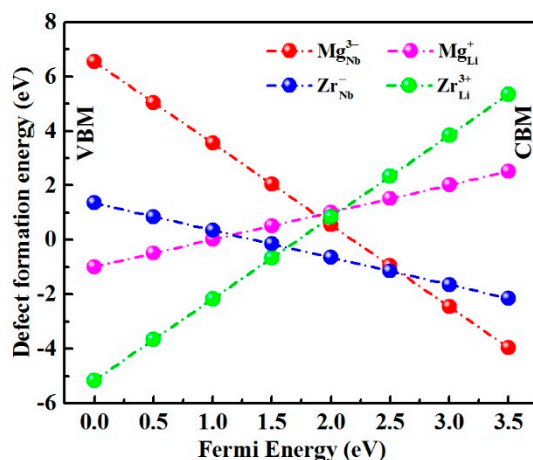


Figure 3. Formation energies of point defects $\text{Mg}_{\text{Li}}^{+}$, $\text{Mg}_{\text{Nb}}^{3-}$, $\text{Zr}_{\text{Li}}^{3+}$, $\text{Zr}_{\text{Nb}}^{-}$ in LN:Mg,Zr crystals. The valance-band maximum and the conduction-band minimum are labelled as VBM and CBM, respectively. Fermi energy (E_F) range corresponds to the fundamental band gap of LN.

In our previous report [19] we employed the OH^{-} absorption spectra and UV-visible absorption spectra to analyze the defects of these doubly co-doped crystals, and the results indicated that the $\text{Mg}_{\text{Li}}^{+} + \text{Zr}_{\text{Nb}}^{-}$ defect clusters exist in crystals. Hence, according to the experimental results and the above calculated results of point defects, three kinds of defect clusters were constructed to find the energetically preferable configuration in LN:Mg,Zr crystals:

1. Zr^{4+} and Mg^{2+} ions only occupy Li-sites, labelled as $\text{Zr}_{\text{Li}}^{3+} + 4\text{V}_{\text{Li}}^{-} + \text{Mg}_{\text{Li}}^{+}$;
2. Zr^{4+} and Mg^{2+} ions replace Nb- and Li-sites, respectively, labelled as $\text{Mg}_{\text{Li}}^{+} + \text{Zr}_{\text{Nb}}^{-}$;
3. Zr^{4+} ions only substitute Nb-sites while Mg^{2+} ions occupy both Li- and Nb-sites, labelled as $\text{Zr}_{\text{Nb}}^{-} + 4\text{Mg}_{\text{Li}}^{+} + \text{Mg}_{\text{Nb}}^{3-}$.

Table 1 shows the calculated defect formation energies, and the $\text{Mg}_{\text{Li}}^{+} + \text{Zr}_{\text{Nb}}^{-}$ defect cluster had the lowest defect formation energy, reflecting that the existence of $\text{Mg}_{\text{Li}}^{+} + \text{Zr}_{\text{Nb}}^{-}$ defect cluster in LN:Mg,Zr was reasonable, which is in agreement with that of our previous experimental results.

Table 1. Formation energies of defect clusters in LN:Mg,Zr.

Defect Clusters	$\text{Zr}_{\text{Li}}^{3+} + 4\text{V}_{\text{Li}}^{-} + \text{Mg}_{\text{Li}}^{+}$	$\text{Mg}_{\text{Li}}^{+} + \text{Zr}_{\text{Nb}}^{-}$	$\text{Zr}_{\text{Nb}}^{-} + 4\text{Mg}_{\text{Li}}^{+} + \text{Mg}_{\text{Nb}}^{3-}$
Formation energy (eV)	12.856	1.064	4.613

3.3. Charge States of LN:Mg,Zr

The partial density of states (PDOS) of LN:Mg,Zr was calculated with the aforementioned optimal $\text{Mg}_{\text{Li}}^{+} + \text{Zr}_{\text{Nb}}^{-}$ model, as shown in Figure 4a. Moreover, according to the $3\text{Mg}_{\text{Li}}^{+} + \text{Mg}_{\text{Nb}}^{3-}$ defect model [26], the calculated PDOS of LN:Mg is described in Figure 4b for comparison. The PDOS clearly showed the DOS of each atom in the LN:Mg,Zr crystals, and the highest occupied valence band exhibits mainly O-2p features, whereas the lowest unoccupied conduction band mainly consists of Nb-4d electrons, meaning that the band gap of LN is determined by the transition energy of an electron transition from O^{2-} 2p-state to Nb^{5+} 4d-state, consistent with the widely accepted results [28].

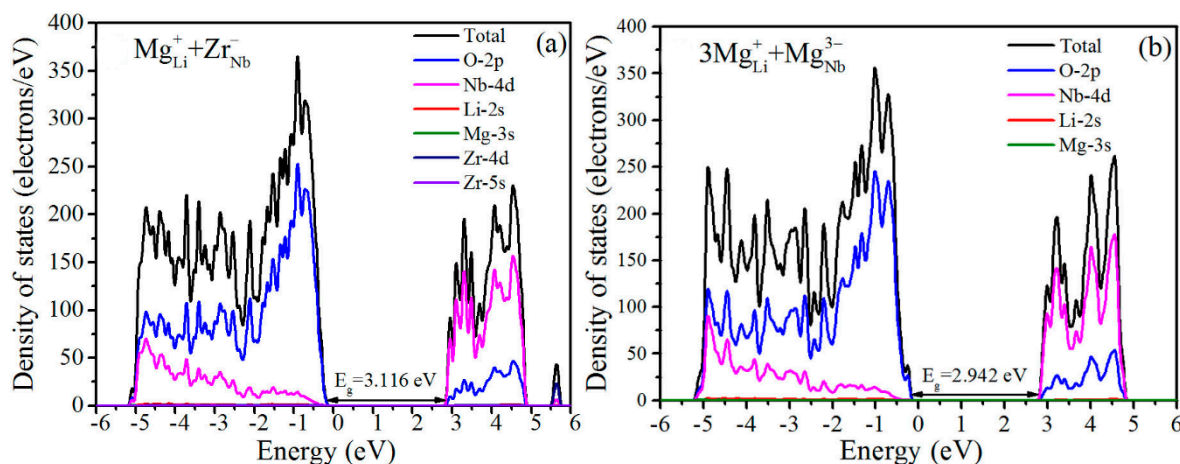


Figure 4. Density of states for (a) LN:Mg,Zr based on the $\text{Mg}_{\text{Li}}^+ + \text{Zr}_{\text{Nb}}^-$ defect model. For comparison, that of (b) LN:Mg based on the $3\text{Mg}_{\text{Li}}^+ + \text{Mg}_{\text{Nb}}^{3-}$ cluster is also presented.

Moreover, it can also be seen that the density of states of O-2p and Nd-4d in LN:Mg,Zr exhibit a distinctly decreased DOS at valence band maximum (VBM) and conduction band minimum (CBM), respectively, which elucidates the reduction of charge carriers in crystals [29]. The enhancement of resistance against UV optical damage of LN:Zr is considered as the reduction of UV photorefractive centers such as $\text{O}^{2-/-}$ near Zr_{Nb}^- [11,30]. It knows by the calculated DOS that the charge density of O-2p of LN:Mg is reduced dramatically by ZrO_2 co-doping, which signifies that the UV photorefractive center $\text{O}^{2-/-}$ of LN:Mg,Zr is sharply decreased. Moreover, the band gap of LN:Mg,Zr is calculated to be about 3.116 eV, which is significantly greater than that of LN:Mg (2.942 eV), and the increase in band gap of LN:Mg,Zr makes charge carriers excitation from $\text{O}^{2-/-}$ more difficult, which powerfully proves the above analysis and further confirms the theoretical calculation corresponding to the experiment results. Based on the analyses above, we state that the reduction in the number of UV photorefractive canters $\text{O}^{2-/-}$ and the increased band gap together result in the high resistance against UV optical damage of LN:Mg,Zr.

4. Conclusions

In summary, we have investigated the resistance against ultraviolet damage and electronic structures of LN:Mg co-doping with ZrO_2 by experiment and first-principles calculations. It is found that ZrO_2 co-doping greatly improves the ultraviolet damage resistance of LN:Mg. Meantime, first-principles calculations elucidated that the enhancement of resistance against UV damage of LN:Mg by co-doping ZrO_2 is caused by both the increased band gap and the reduced ultraviolet photorefractive center $\text{O}^{2-/-}$. This knowledge may open avenues to expand the nonlinear optical applications of LN:Mg to the UV region, and it can be an important candidate material for UV frequency conversion.

Author Contributions: Conceptualization, H.L. and Z.F.; methodology, T.K. and W.W.; investigation, T.K. and W.W.; data curation, Y.L. and H.K.; writing—original draft preparation, T.K. and H.L.; writing—review and editing, W.W., Y.L. and H.K.; All authors have read and agreed to the published version of the manuscript.

Funding: This research was funded by the Science Foundation of Henan University of Technology (2018BS058) and the Natural Science Project in Henan Province Department of Education (21B140004).

Institutional Review Board Statement: Not applicable.

Informed Consent Statement: Not applicable.

Data Availability Statement: The data presented in this study are available from the corresponding author on reasonable request.

Conflicts of Interest: The authors declare no conflict of interest.

References

- Carrascosa, M.; García-Cabañes, A.; Jubera, M.; Ramiro, J.B.; Agulló-López, F. LiNbO₃: A photovoltaic substrate for massive parallel manipulation and patterning of nano-objects. *Appl. Phys. Rev.* **2015**, *2*, 040605. [\[CrossRef\]](#)
- Kong, Y.; Bo, F.; Wang, W.; Zheng, D.; Liu, H.; Zhang, G.; Rupp, R.; Xu, J. Recent progress in lithium niobate: Optical damage, defect simulation, and on-chip devices. *Adv. Mater.* **2019**, *32*, e1806452. [\[CrossRef\]](#) [\[PubMed\]](#)
- Krogen, P.; Suchowski, H.; Liang, H.; Flemens, N.; Hong, K.H.; Kärtner, F.X.; Moses, J. Generation and multi-octave shaping of mid-infrared intense single-cycle pulses. *Nat. Photonics* **2017**, *11*, 222–227. [\[CrossRef\]](#)
- Ashkin, A.; Boyd, G.D.; Dziedzic, J.M.; Smith, R.G.; Ballman, A.A.; Levinstein, J.J.; Nassau, K. Optically-induced refractive index inhomogeneities in LiNbO₃ and LiTaO₃. *Appl. Phys. Lett.* **1966**, *9*, 72–74. [\[CrossRef\]](#)
- Zhong, G.; Jin, J.; Wu, Z. Measurement of optically induced refractive index damage of lithium niobate doped with different concentrations of MgO. *J. Opt. Soc. Am.* **1980**, *70*, 631–635.
- Bryan, D.A.; Gerson, R.; Tomaschke, H.E. Increased optical damage resistance in lithium niobate. *Appl. Phys. Lett.* **1984**, *44*, 847–849. [\[CrossRef\]](#)
- Escalé, M.R.; Sergeyev, A.; Geiss, R.; Grange, R. Nonlinear mode switching in lithium niobate nanowaveguides to control light directionality. *Opt. Express* **2017**, *25*, 3013–3023. [\[CrossRef\]](#)
- Li, G.; Chen, Y.; Jiang, H.; Chen, X. Broadband sum-frequency generation using D₃₃ in periodically poled LiNbO₃ thin film in the telecommunications band. *Opt. Lett.* **2017**, *42*, 939–942. [\[CrossRef\]](#) [\[PubMed\]](#)
- Xu, J.; Zhang, G.; Li, F.; Zhang, X.; Sun, Q.; Liu, S.; Song, F.; Kong, Y.; Chen, X.; Qiao, H.; et al. Enhancement of ultraviolet photorefractive in highly magnesium-doped lithium niobate crystals. *Opt. Lett.* **2000**, *25*, 129–131. [\[CrossRef\]](#) [\[PubMed\]](#)
- Kong, Y.; Liu, S.; Zhao, Y.; Liu, H.; Chen, S.; Xu, J. Highly optical damage resistant crystal: Zirconium-oxide-doped lithium niobate. *Appl. Phys. Lett.* **2007**, *91*, 081908. [\[CrossRef\]](#)
- Liu, F.C.; Kong, Y.F.; Li, W.; Liu, H.D.; Liu, S.G.; Chen, S.L.; Zhang, X.Z.; Rupp, R.; Xu, J.J. High resistance against ultraviolet photorefractive in zirconium-doped lithium niobate crystals. *Opt. Lett.* **2010**, *35*, 10–12. [\[CrossRef\]](#)
- Kovács, L.; Szaller, Z.; Lengyel, K.; Péter, A.; Hajdara, I.; Mandula, G.; Pálfalvi, L.; Hebling, J. Photorefractive damage resistance threshold in stoichiometric LiNbO₃:Zr crystals. *Opt. Lett.* **2013**, *38*, 2861–2864. [\[CrossRef\]](#)
- Nava, G.; Minzioni, P.; Yan, W.B.; Parravicini, J.; Grando, D.; Musso, E.; Cristiani, I.; Argiolas, N.; Bazzan, M.; Ciampolillo, M.V.; et al. Zirconium-doped lithium niobate: Photorefractive and electro-optical properties as a function of dopant concentration. *Opt. Mater. Express* **2011**, *1*, 270–277. [\[CrossRef\]](#)
- Bhatt, R.; Bhaumik, I.; Ganesamoorthy, S.; Bright, R.; Soharab, M.; Karnal, A.; Gupta, P. Control of intrinsic defects in lithium niobate single crystal for optoelectronic applications. *Crystals* **2017**, *7*, 23. [\[CrossRef\]](#)
- Kong, Y.; Liu, F.; Tian, T.; Liu, S.; Chen, S.; Rupp, R.; Xu, J. Fast responsive nonvolatile holographic storage in LiNbO₃ triply doped with Zr, Fe, and Mn. *Opt. Lett.* **2009**, *34*, 3896–3898. [\[CrossRef\]](#) [\[PubMed\]](#)
- Riscob, B.; Bhatt, R.; Vijayan, N.; Bhaumik, I.; Ganesamoorthy, S.; Wahab, M.A.; Rashmi; Bhagavannarayana, G. Structural, optical and thermal properties of Zr-Fe co-doped congruent LiNbO₃ single crystals. *J. Appl. Crystallogr.* **2013**, *46*, 601–609. [\[CrossRef\]](#)
- Qian, Y.; Wang, R.; Wang, B.; Xu, C.; Xing, L.; Xu, Y. Highly efficient 1.54 μm emission in Zr/Yb/Er-codoped LiNbO₃ crystal. *Opt. Lett.* **2012**, *37*, 4176–4178. [\[CrossRef\]](#)
- Zhang, D.L.; Yang, X.F.; Zhang, Q.; Wong, W.H.; Yu, D.Y.; Pun, E.Y.B. Near-stoichiometric Ti-diffused LiNbO₃ strip waveguide doped with Zr⁴⁺. *Opt. Lett.* **2015**, *40*, 5307–5310. [\[CrossRef\]](#) [\[PubMed\]](#)
- Kong, T.; Liu, H.; Ge, X.; Qu, D.; Liu, S.; Chen, S.; Zhang, L.; Kong, Y.; Rupp, R.; Xu, J. Room temperature 90° phase-matching in zirconium and magnesium co-doped lithium niobate crystals. *Sci. Rep.* **2018**, *8*, 3865. [\[CrossRef\]](#) [\[PubMed\]](#)
- Yamamoto, J.K.; Kitamura, K.; Iyi, N.; Kimura, S.; Furukawa, Y.; Sato, M. Increased optical damage resistance in Sc₂O₃-doped LiNbO₃. *Appl. Phys. Lett.* **1992**, *61*, 2156. [\[CrossRef\]](#)
- Kogelnik, H. Coupled wave theory for thick hologram gratings. *Bell Syst. Tech. J.* **1969**, *48*, 2909–2947. [\[CrossRef\]](#)
- Perdew, J.P.; Burke, K.; Ernzerhof, M. Generalized gradient approximation made simple. *Phys. Rev. Lett.* **1996**, *77*, 3865. [\[CrossRef\]](#)
- Xu, H.; Lee, D.; He, J.; Sinnott, S.B.; Gopalan, V.; Dierolf, V.; Phillpot, S.R. Stability of intrinsic defects and defect clusters in LiNbO₃ from density functional theory calculations. *Phys. Rev. B* **2008**, *78*, 174103. [\[CrossRef\]](#)
- Monkhorst, H.J.; Pack, J.D. Special points for Brillouin-zone integrations. *Phys. Rev. B* **1976**, *13*, 5188–5192. [\[CrossRef\]](#)
- Li, Q.; Wang, B.; Woo, C.H.; Wang, H.; Wang, R. First-principles study on the formation energies of intrinsic defects in LiNbO₃. *J. Phys. Chem. Solids* **2007**, *68*, 1336–1340. [\[CrossRef\]](#)
- Li, Y.; Li, L.; Cheng, X.; Zhao, X. Microscopic properties of Mg in Li and Nb Sites of LiNbO₃ by First-Principle Hybrid Functional: Formation and related optical properties. *J. Phys. Chem. C* **2017**, *121*, 8968–8975. [\[CrossRef\]](#)
- Li, L.; Li, Y.; Zhao, X. Hybrid density functional theory insight into the stability and microscopic properties of Bi-doped LiNbO₃: Lone electron pair effect. *Phys. Rev. B* **2017**, *96*, 115118. [\[CrossRef\]](#)
- Földvári, I.; Polgár, K.; Voszka, R.; Balasanyan, R.N. A simple method to determine the real composition of LiNbO₃ crystals. *Cryst. Res. Technol.* **1984**, *19*, 1659–1661. [\[CrossRef\]](#)
- Liang, L.; Lei, F.; Gao, S.; Sun, Y.; Jiao, X.; Wu, J.; Qamar, S.; Xie, Y. Single unit cell Bismuth Tungstate layers realizing robust solar CO₂ reduction to methanol. *Angew. Chem. Int. Ed.* **2015**, *54*, 13971–13974. [\[CrossRef\]](#)
- Herth, P.; Granzow, T.; Schaniel, D.; Woike, T.; Imlau, M.; Krätzig, E. Evidence for light-induced hole polarons in LiNbO₃. *Phys. Rev. Lett.* **2005**, *95*, 067404. [\[CrossRef\]](#) [\[PubMed\]](#)